

Kinetics of Monolayer Growth

Takashi Uchida¹ and Koh Wada¹

Received December 5, 1990; final March 11, 1991

The kinetics of a monolayer growth is studied using the two-dimensional lattice gas model by means of the path-probability method (PPM) for nonequilibrium phenomena. Kinetic equations for the combined processes of relaxation (adsorption and desorption) and diffusion are derived analytically and solved for the first time in the square approximation of the PPM. Comparison of the square approximation with the point and pair approximations along with Monte Carlo simulation shows the effect of using a larger basic cluster than in the previous studies. When the square approximation is used, the growth rate results are much improved in both cases with and without diffusion and agree well with the Monte Carlo simulations results, except for very small values of the driving force $L = \Delta\mu/k_B T$, where $\Delta\mu$ is the chemical potential difference between the vapor and the solid phase. In the range where the agreement is good, there exists a region where the growth rate R is proportional to $\exp(-c/L)$ with a constant c . This is the feature which is characteristic of two-dimensional nucleation-limited growth.

KEY WORDS: Monolayer growth; cluster variation method (CVM); path probability method (PPM); diffusion process.

1. INTRODUCTION

The cluster variation method (CVM)⁽¹⁾ and the path probability method (PPM)^(2,3) introduced by Kikuchi have been successfully applied to various phenomena occurring on lattice systems in equilibrium and nonequilibrium processes, respectively. The CVM or the PPM provides, systematically, a series of mean-field-type approximations, each of which is characterized by its basic clusters. The point (mean-field) and the pair approximations are the first two of the series and have been studied extensively.⁽⁴⁻⁶⁾ In most cases the results of these approximations were, however, not quantitatively reliable at low temperatures.^(7,8)

Recently, large basic clusters such as tetrahedra and octahedra have

¹ Department of Physics, Faculty of Science, Hokkaido University, Sapporo 060, Japan.

been used in the CVM in the calculation of phase diagrams and these approximations are found to give improved results.⁽⁹⁾ On the other hand, Kikuchi formulated the triangle approximation of the PPM for relaxation (adsorption and desorption) and diffusion processes in the monolayer growth model and the square approximation only for relaxation process,^(10,11) in addition to his previous work with the pair approximation.^(5,6) The resulting kinetic equations, however, lead to questionable results in both cases. Later, Wada *et al.* formulated the triangle approximation on the solid-on-solid (SOS) model^(4,12-16) of crystal growth and obtained improved results compared with the point and pair approximations.^(3,7) In this case, however, the treatment of diffusion process was not based on the triangle approximation in the strict sense.⁽⁷⁾ As far as we know, reasonable results have not yet been obtained for diffusion kinetics with approximations better than the pair one.

In the present paper, we formulate the square approximation of the PPM for the combined processes of relaxation and diffusion in the monolayer growth model. We have succeeded for the first time in obtaining analytic expressions for the kinetic equations for relaxation and diffusion processes. The time evolution of the density of atoms and the crystal growth rate are calculated and the results are compared with those of the point and pair approximations and those of the Monte Carlo (MC) simulation.^(17,18) The present calculation yields improved results compared with the point and pair approximations and agrees well with the MC simulation.

It should be emphasized that the present paper derives the kinetic equations for diffusion process using the square approximation not merely numerically but analytically, contrary to the general expectation. The novel insight for the formulation presented in this paper may be helpful in other problems of interest, such as the correlation factor problem in the tracer diffusion of multicomponent systems.⁽¹⁹⁾

The outline of the present paper is as follows. In Section 2, we give the definition of the monolayer growth model and study its static properties by means of the CVM. In Section 3, we formulate the square approximation of the PPM and derive analytical expressions for the kinetic equations for relaxation and diffusion. In Section 4, we show the results of the numerical integration of the kinetic equations. The last section is devoted to a summary and discussion.

2. THE MODEL AND ITS EQUILIBRIUM PROPERTIES

We consider a monolayer system represented by a two-dimensional square lattice each site of which is either occupied or unoccupied by a solid

atom. The atoms are supplied from the vapor phase (the particle and thermal reservoir) onto the lattice and the adsorbed atoms can evaporate into the vapor phase.

Using the site variable C_i , which takes 1 or 0 according to whether the i th site is occupied or vacant, the Hamiltonian of the monolayer system is defined as

$$H = J \sum_{\langle i,j \rangle} \{C_i(1 - C_j) + C_j(1 - C_i)\} - \Delta\mu \sum_i C_i \quad (2.1)$$

where the first sum runs over all pairs of nearest neighbor sites and the second over all lattice sites. The first term denotes the excess energy ($J > 0$) of atom-vacancy pairs and the second term denotes the energy gain of solid atoms due to the chemical potential difference $\Delta\mu$ between the vapor and the solid phase.

First we examine the static properties of the monolayer system by means of the CVM.⁽¹⁾ In the square approximation of the CVM, the variables $\{x_i\}$, $\{y_i\}$, and $\{z_i\}$ denote, respectively, the probabilities of appearance of configurations of the point, pair, and square clusters shown in Fig. 1. There are normalization and geometrical relations among the state variables:

$$\begin{aligned} 1 &= x_1 + x_2 \\ x_1 &= y_1 + y_2 \\ x_2 &= y_2 + y_3 \\ y_1 &= z_1 + 2z_2 + z_3 \\ y_2 &= z_2 + z_3 + z_4 + z_5 \\ y_3 &= z_3 + 2z_5 + z_6 \end{aligned} \quad (2.2)$$

Because of the relations (2.2), we can choose five variables, x_1 , y_2 , z_2 , z_3 , and z_5 , hereafter as independent state variables.

The grand potential Ω of the system can be written as a function of independent state variables. From the Hamiltonian H in (2.1), the internal energy E is written as

$$E = JzNy_2 - \Delta\mu Nx_1 \quad (2.3)$$

where z ($=4$) is the coordination number and N is the total number of lattice sites.

The number of possible configurations of the system with a set of state variables $\{x_i, y_i, z_i\}$ is calculated in the present approximation as⁽¹⁾

$$W_0 = \frac{[\prod_k (y_k N)^{\beta_k}]^2}{\prod_i (x_i N)! \prod_j (z_j N)!^{y_j}} \quad (2.4)$$

where β_k and γ_j are the numbers of the pair and square cluster configurations with the same probability of appearance, respectively (see Fig. 1). These numbers come from the fact that equivalent cluster configurations appear because of the symmetry of the system. We call them the symmetry number. Since the entropy S is written as $S = k_B \ln W_0$, the grand potential Ω is constructed from the energy E and the entropy S :

$$\Omega/(Nk_B T) = zKy_2 - Lx_1 + \sum_i x_i \ln x_i + \sum_j \gamma_j z_j \ln z_j - 2 \sum_k \beta_k y_k \ln y_k \quad (2.5)$$

where $L = \Delta\mu/k_B T$, $K = J/k_B T$, and Stirling's formula $N! = N \ln N - N$ have been used. L is often called the driving force in the crystal growth problem since it controls the density of atoms in the monolayer. The thermodynamic equilibrium state of the system corresponds to the minimum of the grand potential Ω .

point	prob.
●	x_1
○	x_2

pair	prob.	β
●—●	y_1	1
●—○	y_2	2
○—○	y_3	1

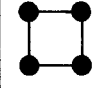
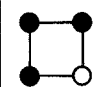
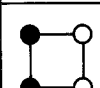
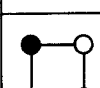

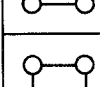
square	prob.	γ
	z_1	1
	z_2	4
	z_3	4
	z_4	2
	z_5	4
	z_6	1

Fig. 1. Cluster configurations and definitions of state variables. β and γ denote the symmetry numbers.

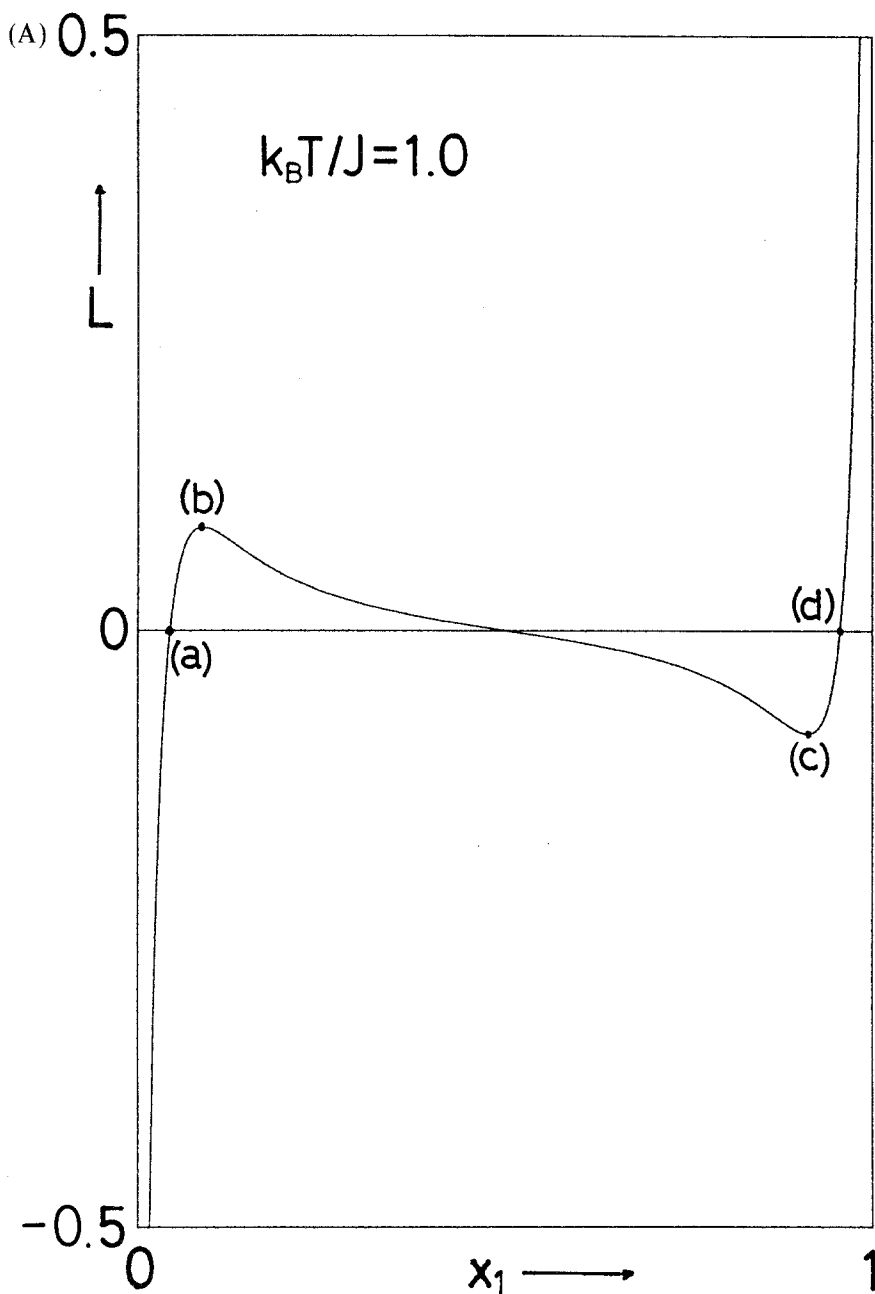


Fig. 2. (A) Isothermal curve in the x_1 vs. L plane at $T < T_c^{(sq)}$ ($k_B T_c^{(sq)}/J \cong 1.213$). There is a van der Waals-type loop (a)-(b)-(c)-(d)-(a) in which the coexistence line (a)-(d) represents stable equilibrium states and the segments (a)-(b) and (c)-(d) represent metastable states, while the states in the segment (b)-(c) are thermodynamically unstable. (B) Isothermal curve in the x_1 vs. L plane at $T > T_c^{(sq)}$. There are no unstable or metastable states.

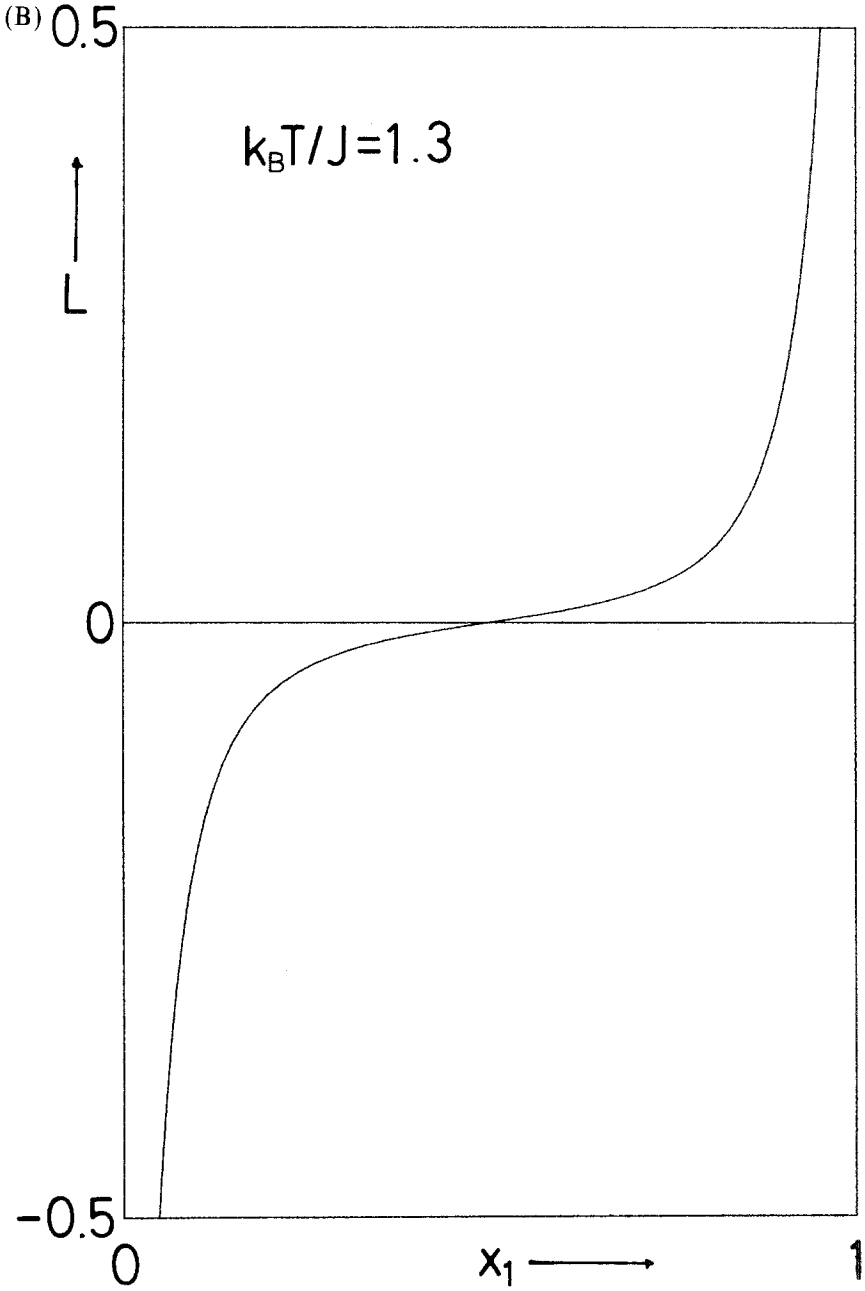


Fig. 2. (Continued)

In a special case with $L=0$, this system undergoes a second-order phase transition if we change the temperature T across the critical temperature T_c . We obtain the value of T_c in the square approximation⁽¹⁾ as

$$k_B T_c^{(sq)}/J = 1/\ln[(45 + 17^{1/2})/4] \cong 1.213$$

The equations of state of the system are determined by the extremum condition of Ω with respect to independent state variables and can be represented as the isotherms in the x_1 vs. L plane as shown in Fig. 2a and 2b.

Below the critical temperature T_c , the isotherm in the x_1 vs. L plane has the van der Waals type loop (Fig. 2a), while above T_c there is no such loop in the isotherm (Fig. 2b).

In the loop (a)–(b)–(c)–(d)–(a) in Fig. 2a, the coexistence line (a)–(d) represents thermodynamically stable equilibrium states in which the grand potential Ω is a minimum. The states between the points (b) and (c) are unstable, since the density x_1 cannot decrease (increase) when the driving force L increases (decreases). The states represented by the segments

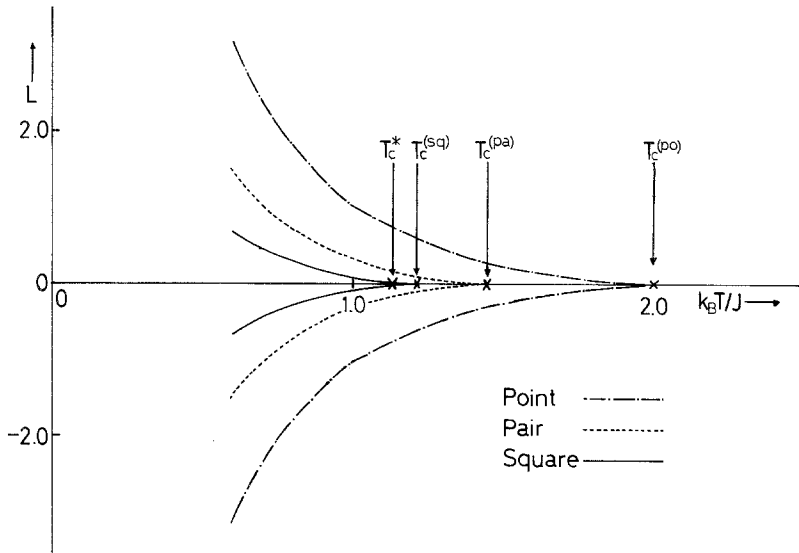


Fig. 3. Spinodal curves in the L vs. $k_B T/J$ plane for the point, pair, and square approximations. The spinodal curve approaches to the coexisting line ($L=0$) as the basic cluster becomes large. T_c^* , $T_c^{(sq)}$, $T_c^{(pa)}$, and $T_c^{(po)}$ denote the critical temperatures of the exact solution, the square approximation, the pair approximation, and the point approximation of the two-dimensional lattice gas model, respectively.

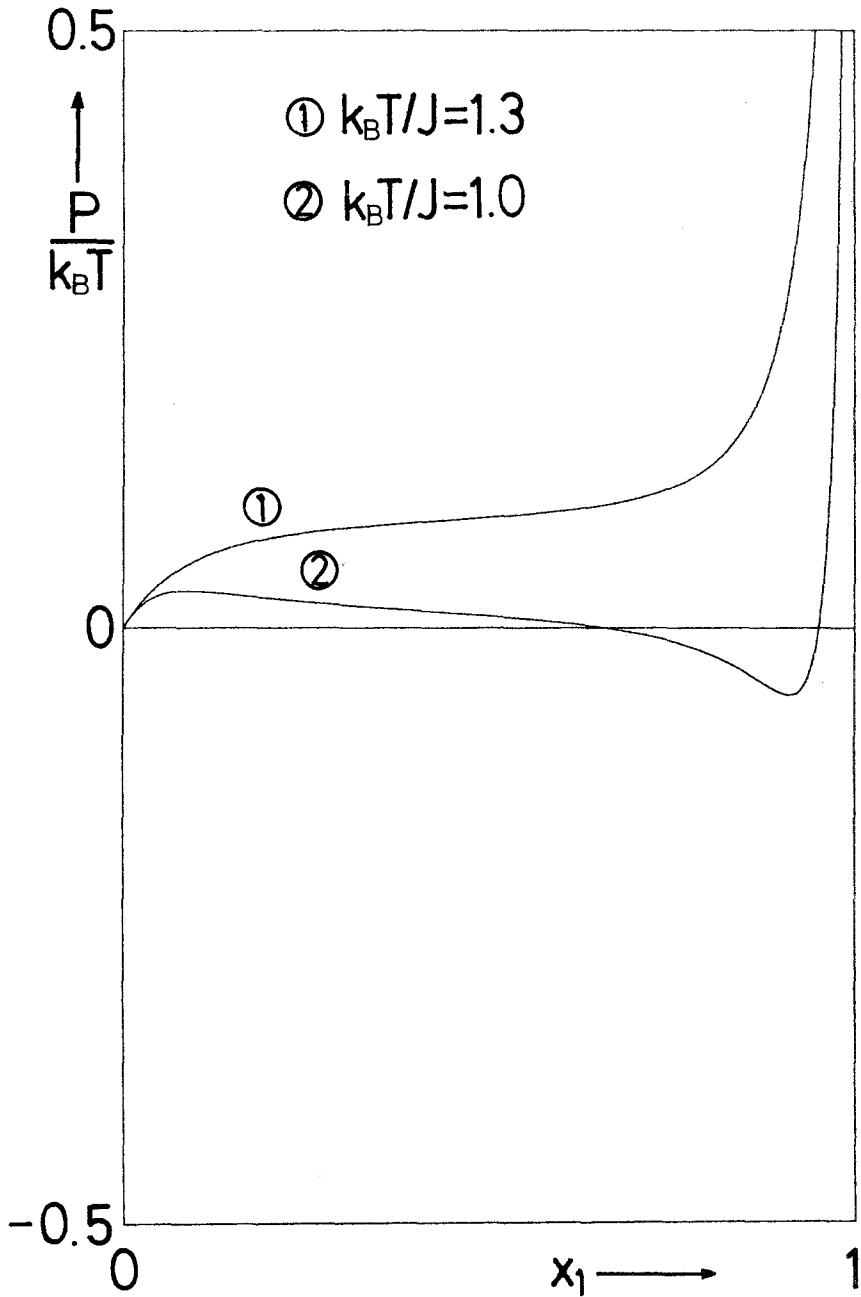


Fig. 4. Isothermal curves ① and ② in the x_1 vs. $P/k_B T$ (density–pressure) plane for $T > T_c$ and for $T < T_c$, respectively, in the square approximation.

(a)–(b) and (c)–(d), on the other hand, are metastable states in which the grand potential Ω takes a local minimum value, but not the true minimum.

The points (b) and (c) at which the state of the system becomes unstable are called spinodal points. At each temperature below T_c , there is a critical driving force L_c corresponding to the spinoidal point (b) [(c)] below (above) which metastable states exist. In Fig. 3, the spinodal curve (which is made up of spinodal points for various temperatures) for the square approximation is shown along with those of the point and pair approximations. We can see that as the approximation is improved, the critical point approaches the exact critical point and the spinodal curve shrinks toward the coexistence line ($L=0$). We will see later that these static properties of the system are closely related to the kinetic properties.

For reference, we also show isotherms in the $P/k_B T$ vs. x_1 plane (P being the pressure), since what we can control in practice is not L , but P (Fig. 4). The pressure P is given by the thermodynamic relation $\Omega = -PV$, where $V = Nv$ ($v = a^2$ with lattice spacing a) is the size of the system. The qualitative features of the curves are the same as those in the x_1 vs. L plane.

3. KINETIC EQUATIONS

We derive kinetic equations for independent state variables in the square approximation of the PPM. Since we consider here the time evolution of the state of the system, each state variable is now a function of time. In addition to the state variables, we introduce variables called path variables each of which connects two states at t and $t + \Delta t$ of a cluster. The path variables for relaxation process are written as $\{X_{ij}(t, t + \Delta t)\}$, $\{Y_{ij}(t, t + \Delta t)\}$, and $\{Z_{ij}(t, t + \Delta t)\}$, the capital letters X , Y , and Z representing the point, pair, and square clusters, respectively. Similarly, the path variables for the diffusion process are written as $\{X_{ijD}(t, t + \Delta t)\}$, $\{Y_{ijD}(t, t + \Delta t)\}$, and $\{Z_{ijD}(t, t + \Delta t)\}$, where the subscript D is added to distinguish diffusion from relaxation. Here one comment should be in order. We use the term “relaxation process” for single-site processes (adsorption and desorption) and “diffusion process” for two-site processes. The path variable with subscripts i and j denotes the joint probability that the cluster takes the i th configuration at t and the j th configuration at $t + \Delta t$ through specified kinetics (relaxation or diffusion). The ways of numbering cluster configurations in the path variables are the same as those used in the state variables (see Fig. 1). Some examples of the path variables and the changes of cluster configurations are presented in the Appendix. In the following, we omit the arguments t and $t + \Delta t$ from the path variables, for simplicity. There are geometrical relations among the path variables similar to those between the state variables. The state

variables at the initial time t and the latter time $t + \Delta t$ are easily obtained from the path variables, since the path variables are the joint probability functions connecting the cluster configurations at t and $t + \Delta t$.

We now write down the path probability function, which plays the same role in the PPM as the free energy (the grand potential in the present case) does in the CVM. By the term "path" we mean a change of state of the system in a short time interval Δt . The path probability function $P(\{X_{ij}, Y_{ij}, Z_{ij}, X_{ijD}, Y_{ijD}, Z_{ijD}\})$ is the conditional probability that any one of the paths specified by the set of path variables $\{X_{ij}, Y_{ij}, Z_{ij}, X_{ijD}, Y_{ijD}, Z_{ijD}\}$ is realized when the initial state $\{x_i(t), y_i(t), z_i(t)\}$ is given. It consists of three factors.

The first is a kinetic factor given by

$$P1 = (\theta_R \Delta t)^{NX_{21}} (\theta_R \Delta t)^{NX_{12}} (\theta_D \Delta t)^{NzY_{2D}} (1 - \Theta(t) \Delta t)^{NX_{11}} (1 - \Theta(t) \Delta t)^{NX_{22}} \quad (3.1)$$

where θ_R and θ_D are the microscopic characteristic rates for relaxation and diffusion, respectively. Here $1 - \Theta(t) \Delta t$ is the probability that no adsorption, desorption, or diffusion occurs at a lattice site in Δt for given values of K and L and, if needed, $\Theta(t)$ can be determined self-consistently.⁽²⁰⁾

The second is a Boltzmann-like factor:

$$P2 = \exp(-\Delta E/k_B T) \quad (3.2)$$

where the energy change ΔE in Δt is given by

$$\begin{aligned} \Delta E = & -N\Delta\mu X_{21} + 4NJ(Y_{12} - Y_{23}) \\ & + 4NJ(2Y_{12D1} + Y_{12D2} - 2Y_{23D1} - Y_{23D2}) \end{aligned} \quad (3.3)$$

The first term in (3.3) denotes the energy change in adsorption due to the chemical potential difference $\Delta\mu$. It is assumed that the probability of adsorption does not depend on the adsorption site. The second term denotes the energy change due to desorption. The third term accounts for the energy change in the diffusion process which involves a migration of an atom from an initial site to one of its nearest neighboring sites. It is also assumed that the probability of diffusion does not depend on the final site of the atom.

The third factor $P3$,⁽²⁾ which is related to the path entropy, is the number of equivalent paths with a set of path variables $\{X_{ij}, Y_{ij}, Z_{ij}, X_{ijD}, Y_{ijD}, Z_{ijD}\}$ starting from the state $\{x_i(t), y_i(t), z_i(t)\}$:

$$\begin{aligned} P3 &= \frac{W}{W_0} \\ &= \frac{\{\text{bond}\}_{\Delta t}^2}{\{\text{point}\}_{\Delta t} \{\text{square}\}_{\Delta t}} \bigg/ \frac{\{\text{bond}\}_t^2}{\{\text{point}\}_t \{\text{square}\}_t} \end{aligned} \quad (3.4)$$

where

$$\begin{aligned}
 \{\text{point}\}_{\Delta t} &= \prod_{i,j} (X_{ij}N)! \prod_{k,l} (X_{klD}N)!^{A_{klD}} \\
 \{\text{bond}\}_{\Delta t} &= \prod_{i,j} (Y_{ij}N)!^{B_{ij}} \prod_{k,l} (Y_{klD}N)!^{B_{klD}} \\
 \{\text{square}\}_{\Delta t} &= \prod_{i,j} (Z_{ij}N)!^{G_{ij}} \prod_{k,l} (Z_{klD}N)!^{G_{klD}} \\
 \{\text{point}\}_t &= \prod_i (x_iN)! \\
 \{\text{bond}\}_t &= \prod_i (y_iN)!^{\beta_i} \\
 \{\text{square}\}_t &= \prod_i (z_iN)!^{\gamma_i}
 \end{aligned} \tag{3.5}$$

Here A_{ijD} , B_{ij} , B_{ijD} , G_{ij} , and G_{ijD} are the symmetry numbers for the path variables for the point, pair, and square clusters, respectively, similar to those of state variables. The list of symmetry numbers for the path variables is presented in Table I of the Appendix. Note that W_0 is the combinatorial expression (2.4) used in the CVM, and in W the state variables of W_0 are replaced by the corresponding path variables.

The product P of the three factors P_1 , P_2 , and P_3 gives the path probability function of the system. Its logarithmic form is given by

$$\begin{aligned}
 N^{-1} \ln P &= 2 \sum_{ij} B_{ij} Y_{ij} \ln Y_{ij} - \sum_{kl} G_{kl} Z_{kl} \ln Z_{kl} - \sum_{mn} X_{mn} \ln X_{mn} \\
 &+ 2 \sum_{ij} B_{ijD} Y_{ijD} \ln Y_{ijD} - \sum_{kl} G_{klD} Z_{klD} \ln Z_{klD} \\
 &- \sum_{mn} A_{mnD} X_{mnD} \ln X_{mnD} \\
 &+ (X_{11} + X_{22}) \ln(1 - \Theta \Delta t) + (X_{21} + X_{12}) \ln(\theta_R \Delta t) + 4 Y_{22D} (\theta_D \Delta t) \\
 &+ L X_{21} - 4K(Y_{12} - Y_{23}) - 4K(2Y_{12D1} + Y_{12D2} - 2Y_{23D1} - Y_{23D2}) \\
 &- 2 \sum_i \beta_i y_i \ln y_i + \sum_j \gamma_j z_j \ln z_j + \sum_k x_k \ln x_k
 \end{aligned} \tag{3.6}$$

The kinetic equations of the system are obtained from the most probable path derived by minimizing the path probability function P with respect to independent path variables. The differentiation of (3.6) with respect to them leads to 28 algebraic equations, which are separated into

three groups; six equations for adsorption (A), six equations for desorption (B), and 16 equations for diffusion (C). In terms of state variables and given parameters such as L , K , θ_R , θ_D , and Δt , they are analytically solved to give the following expressions for the independent path variables. These equations have self-explanatory intuitive interpretations.

(A) Adsorption

$$\frac{Y_{21}}{y_2} = \frac{Y_{32}}{y_3} = \frac{Z_{21}}{z_2} = \frac{Z_{32}}{z_3} = \frac{Z_{42}}{z_4} = \frac{Z_{54}}{z_5} = e^{L\theta_R \Delta t} \quad (3.7)$$

(B) Desorption

$$\begin{aligned} \frac{Y_{12}}{(1/H)w_1 + w_3} &= \frac{Y_{23}}{w_3 + Hw_5} = \frac{Z_{23}}{z_2} = H \frac{Z_{12}}{z_1} = H \frac{Z_{24}}{z_2} = \frac{Z_{45}}{Hz_4} \\ &= \frac{X_{12}}{(1/H)w_1 + 2w_3 + Hw_5} \end{aligned} \quad (3.8)$$

$$X_{12} = x_1 \theta_R \Delta t \left[\frac{1}{2} \left(\frac{w_1}{y_1 e^K} + \frac{w_5}{y_2 e^{-K}} + D \right) \right]^4$$

with

$$D = \left[\left(\frac{w_1}{y_1 e^K} - \frac{w_5}{y_2 e^{-K}} \right)^2 + \frac{4w_3^2}{y_1 y_2} \right]^{1/2}$$

$$H = \frac{y_1 e^K}{2w_3} \left(\frac{w_5}{y_2 e^{-K}} - \frac{w_1}{y_1 e^K} + D \right)$$

$$w_1 = z_1 + z_2, \quad w_3 = z_2 + z_3, \quad w_5 = z_4 + z_5$$

(C) Diffusion

$$Y_{22D} = X_{12D} = X_{12D} = \theta_D \Delta t \left(\frac{x_1}{y_2} \right) \left(\frac{w_3 + Hw_5}{y_2 e^{-KS}} \right) \left(\frac{S(w_5 t_1 + w_3 t_2)}{y_1 e^K (w_3 + Hw_5)} \right)^2 \quad (3.9)$$

and

$$\frac{Z_{21D}}{z_2} = \frac{Z_{32D}}{z_3} = \frac{Z_{42D}}{z_4} = \frac{Z_{54D}}{z_5} = \frac{Z_{32D1}}{z_3} = \frac{E_{32D2}}{z_3} = \frac{Y_{21D1}}{y_2} = \frac{Y_{21D2}}{y_2} = \frac{Y_{22D}}{x_2}$$

$$\frac{HZ_{12D}}{z_1} = \frac{HZ_{24D}}{z_2} = \frac{Z_{23D1}}{z_2} = \frac{Z_{23D2}}{z_2} = \frac{Z_{45D}}{Hz_4} = \frac{Y_{22D}}{S}$$

$$\frac{Y_{12D1}}{(1/H)w_1 + w_3} = \frac{Y_{12D2}}{(1/H)w_1 + w_3} = \frac{Y_{22D}}{S}, \quad \frac{Z_{22D}}{z_2} = \frac{t_2 Y_{22D}}{w_5 t_1 + w_3 t_2}$$

with

$$S = \frac{1}{H} w_1 + 2w_3 + Hw_5, \quad t_1 = y_1 e^K (w_3 + Hw_5), \quad t_2 = y_2 e^{-K} (w_1 + Hw_3)$$

By making use of the fact that each state variable is written as a linear combination of path variables, we can obtain the kinetic equations for independent state variables:

$$\begin{aligned} \frac{dx_1}{dt} &= \theta_R [e^L x_2 - x_1 \lambda_e^4] \\ \frac{dy_2}{dt} &= \theta_R \left[(y_3 - y_2) e^L + x_1 \frac{Hw_5 - (1/H)w_1}{R} \lambda_e^4 \right] \\ &\quad + 3\theta_D \left[\frac{y_3 - y_2}{x_2} - \frac{Hw_5 - (1/H)w_1}{S} \right] \lambda_D \\ \frac{dz_2}{dt} &= \theta_R \left[(2z_3 + z_4 - z_2) e^L - x_1 \frac{2z_2 + (1/H)(z_2 - z_1)}{R} \lambda_e^4 \right] \\ &\quad + 2\theta_D \left[\frac{2z_3 + z_4 - z_2}{x_2} - \frac{2z_2 - (1/H)(z_2 + z_1)}{S} \right] \lambda_D \quad (3.10) \\ \frac{dz_3}{dt} &= 2\theta_R \left[(z_5 - z_3) e^L - x_1 \frac{z_3 - z_2}{R} \lambda_e^4 \right] \\ &\quad + 2\theta_D \left[\frac{2(z_5 - z_3)}{x_2} - \frac{2(z_3 - z_2)}{S} + \frac{2(z_4 t_1 - z_3 t_2)}{w_5 t_1 + w_3 t_2} \right] \lambda_D \\ \frac{dz_5}{dt} &= \theta_R \left[(z_6 - 3z_5) e^L - x_1 \frac{H(z_5 - z_4) - 2z_3}{R} \lambda_e^4 \right] \\ &\quad + 2\theta_D \left[\frac{z_6 - 3z_5}{x_2} - \frac{H(z_5 - z_4) + 2z_3}{S} \right] \lambda_D \end{aligned}$$

where

$$\begin{aligned} \lambda_e &= \frac{1}{2} \left(\frac{w_1}{y_1 e^K} + \frac{w_5}{y_2 e^{-K}} + D \right) \\ \lambda_D &= \frac{Y_{22D}}{\theta_D \Delta t} = \frac{x_1 w_3 + Hw_5}{y_2 y_2 e^{-KS}} \left(\frac{S(w_5 t_1 + w_3 t_2)}{y_1 e^K (w_3 + Hw_5)} \right)^2 \end{aligned}$$

Since the total number of atoms Nx_1 in the monolayer does not change by diffusion, the kinetic equation for x_1 does not involve a diffusion part. The

other kinetic equations consist of relaxation and diffusion parts. The relative influence of diffusion upon relaxation process is measured by the diffusion length X_s ,^(15,18) defined by $X_s = (\theta_D z / \theta_R)^{1/2}$, which represents the mean diffusion distance (in units of lattice constant a) of an isolated atom during its lifetime until desorption occurs.

4. NUMERICAL RESULTS

In order to see the time evolution of the system, we integrate the kinetic equations using the Runge-Kutta method. In Figs. 5 and 6 the time evolution of the density $x_1(t)$ of atoms is shown.

First let us examine the cases for $T < T_c$ without diffusion (Fig. 5a). As stated in Section 2, at $T < T_c$ there is a critical driving force L_c below which metastable states exist. For $L < L_c$, when we start integration from an almost vacant state of the system, the density x_1 increases to the value of the metastable state but does not climb up to the value of the stable equilibrium state (① in Fig. 5a). For $L > L_c$, on the other hand, the density $x_1(t)$ stays initially on a flat portion for a while and then climbs to the final saturation value, which is equal to the stable equilibrium value determined from the equations of state in the CVM (②–⑤ in Fig. 5a). As the driving force L is increased, the initial flat portion and the elapsed time until saturation decrease. In Fig. 5b the results with diffusion length $X_s = 2$ are shown. Although the qualitative features of the curve are the same as in Fig. 5b, the initial flat portion for $L > L_c$ is smaller than in the case without diffusion.

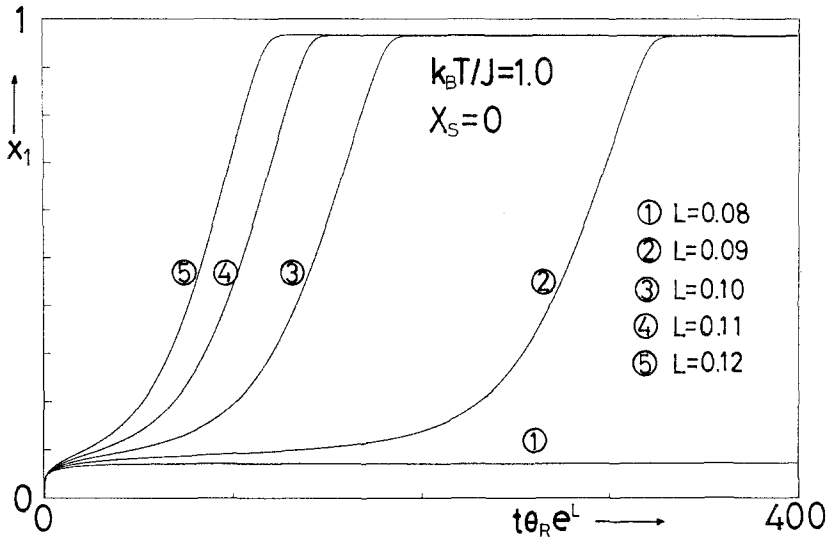
In the case of $T > T_c$, there are no metastable states and hence no critical driving force L_c . For all $L > 0$, the initial flat portion found in Fig. 5a does not exist and the density x_1 increases directly to the final equilibrium value (Fig. 6a). Also in this case the diffusion leads to a faster crystal growth (Fig. 6b).

The reason for the faster crystal growth in the presence of diffusion is that the diffusion tends to bring the system into local equilibrium and thus the rate of evaporation is reduced compared to the case without diffusion. This effect was also discussed in the pair approximation.⁽¹⁵⁾

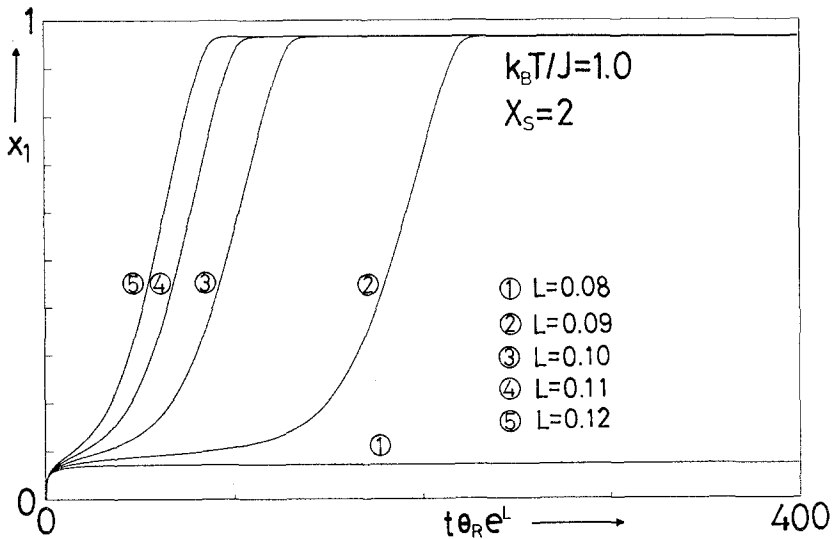
We next examine the dependence of the growth rate R on the driving force L . In the present case the crystal growth rate R is defined as

$$R = \Delta x_1 / \Delta t \quad (4.1)$$

where Δx_1 is the increment of x_1 from the initial, almost zero value to the almost saturated value [$x_1(0) = 1.0 \times 10^{-3}$ to 99.3% of the saturated value] and Δt is the elapsed time. We show in Fig. 7 the dependence of the

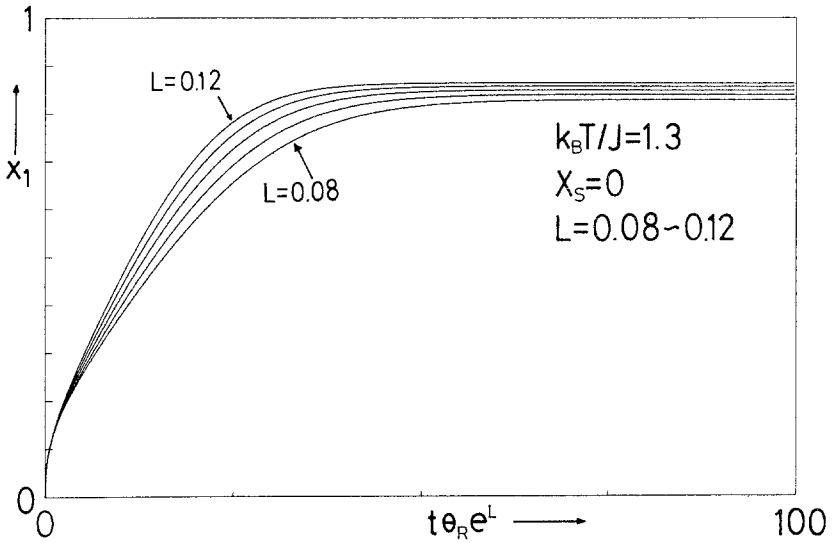


(A)

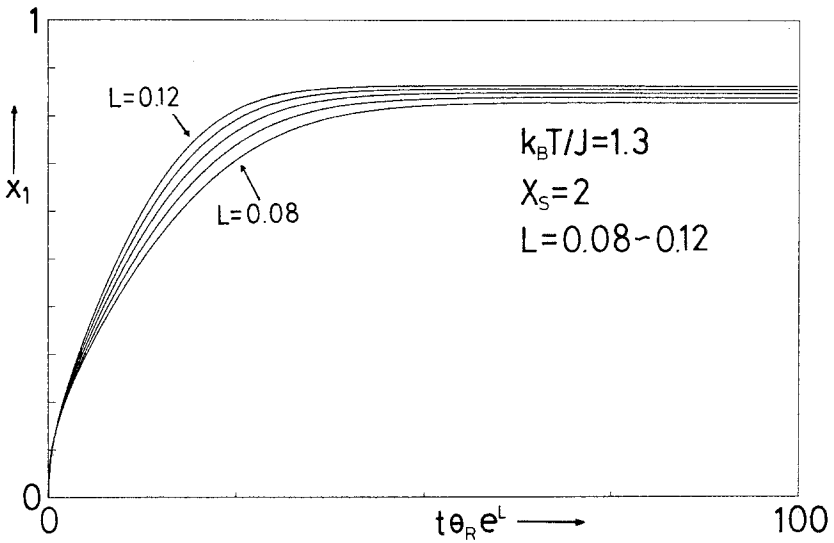


(B)

Fig. 5. (A) The time evolution of the density x_1 of atoms at $T < T_c^{(sq)}$ without diffusion ($X_s=0$). For $L < L_c$, the system is captured in a metastable state (①). For $L > L_c$, the density x_1 stays initially on a flat portion for a while and then climbs up to the final saturation value (② → ⑤). As the driving force L is increased, the initial flat portion and hence the time elapsed until the saturation become shorter. (B) The time evolution of the density x_1 of atoms at $T < T_c^{(sq)}$ with $X_s=2$. This case shows faster growth than in the case without diffusion (A). Diffusion does not change the critical value of the driving force L_c .



(A)



(B)

Fig. 6. (A) The time evolution of the density x_1 of atoms at $T > T_c$ without diffusion ($X_s = 0$). The density x_1 increases directly to the saturation value for all $L > 0$. (B) The time evolution of the density x_1 of atoms at $T > T_c$ with $X_s = 2$. This case shows faster growth than in the case without diffusion (A).

growth rate R on the driving force L at a temperature $k_B T/J=1.0$ ($\langle k_B T_c^{(sq)}/J \cong 1.213$). In this and the following figures, we use the normalized growth rate R/k_0^+ , where k_0^+ is defined by $k_0^+ = \theta_R e^L$. The growth rate data of the point, pair, and square approximation are presented along with those of the Monte Carlo simulations, which we have

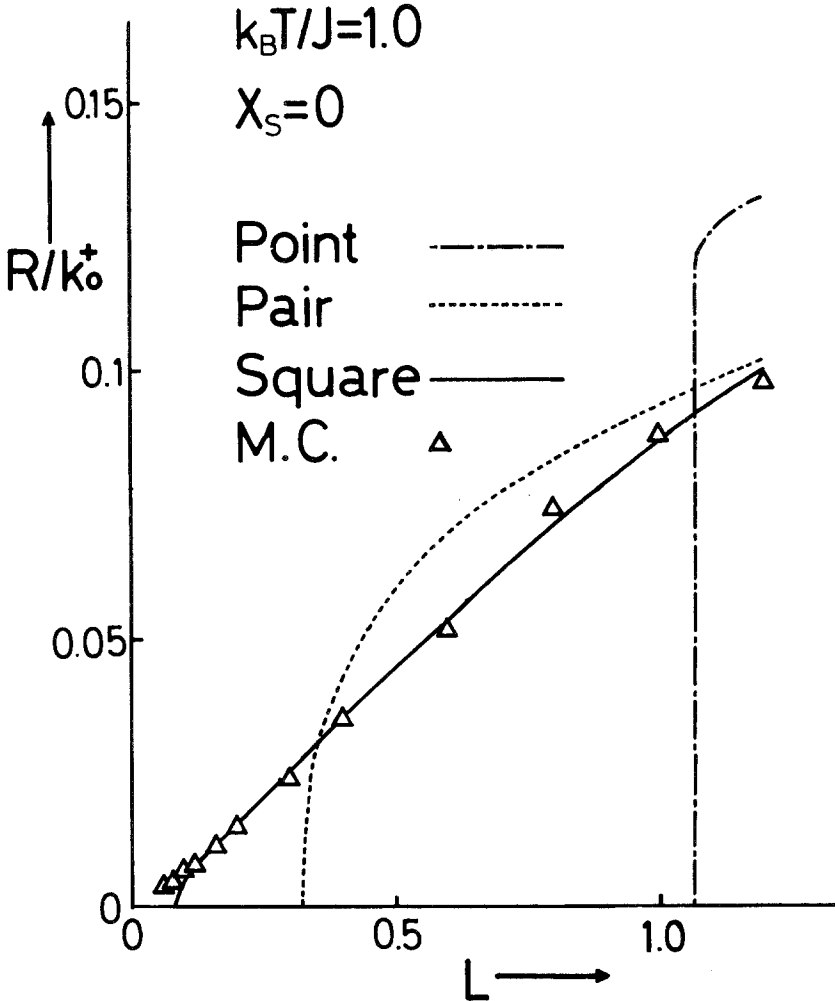


Fig. 7. The growth rate data of the point, pair, and square approximations with L as abscissa are plotted along with the Monte Carlo simulation data (40×40 lattice) at $k_B T/J = 1.0$ ($\langle k_B T_c^{(sq)}/J \cong 1.213$) without diffusion. As the basic cluster becomes large, the growth rate results are improved.

performed according to the method of Gilmer and Bennema.^(17,18) We see that as the basic cluster becomes large, the growth rate results agree better with those of the Monte Carlo simulation. We also see that the unphysical nongrowth region shrinks considerably in the square approximation compared with the point and pair approximations. We note that this result is related to the static result of the CVM in which the region of metastable states shrinks as the approximation improves (see Fig. 3).

In order to see the behavior for small L in detail, the data in Fig. 7 are plotted again in Fig. 8A, in which the vertical axis is $\ln(R/k_0^+)$ and the

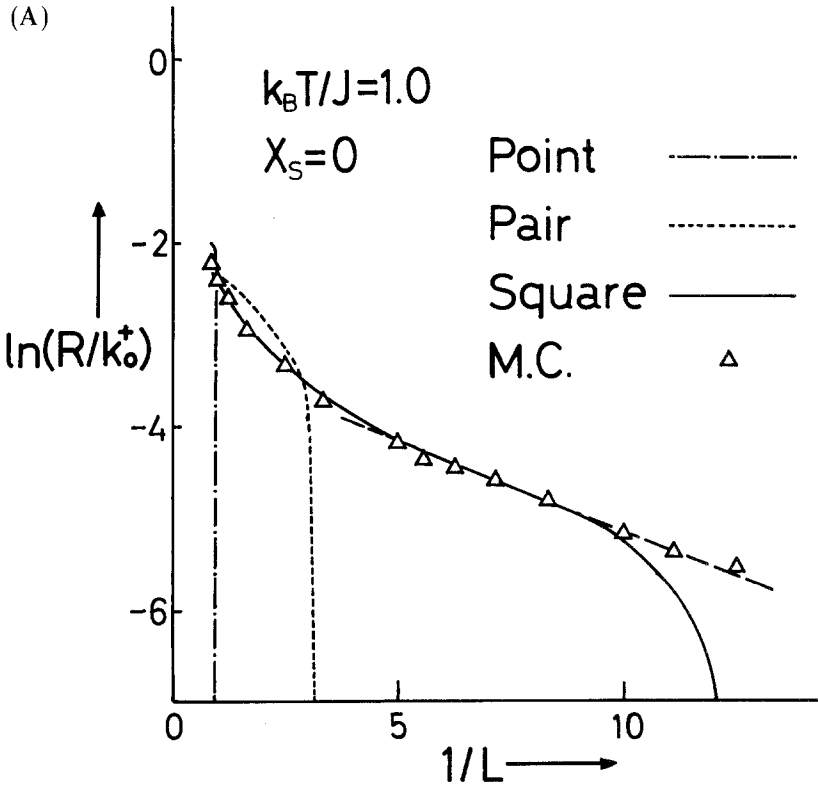


Fig. 8. (A) Semilogarithmic plot of the growth rate data with $1/L$ as abscissa at $k_B T/J = 1.0$ ($\langle k_B T_c^{(sq)}/J \cong 1.213$) without diffusion ($X_s = 0$). The growth rate data of the square approximation are on a linear curve for relatively small L and fit the Monte Carlo simulation data (40×40 lattice), showing the exponential dependence $R = c_0 \exp(-c_1/L)$ (c_0 and c_1 being a constant) of the growth rate R on the driving force L . The linear portion of the square approximation data in this figure corresponds to the range of driving force L from about 0.1 to 0.2 in Fig. 7. (B) Semilogarithmic plot of the growth rate data with $1/L$ as abscissa at $k_B T/J = 1.0$ with $X_s = 2$. The results of the square approximation show the same features as those in (A).

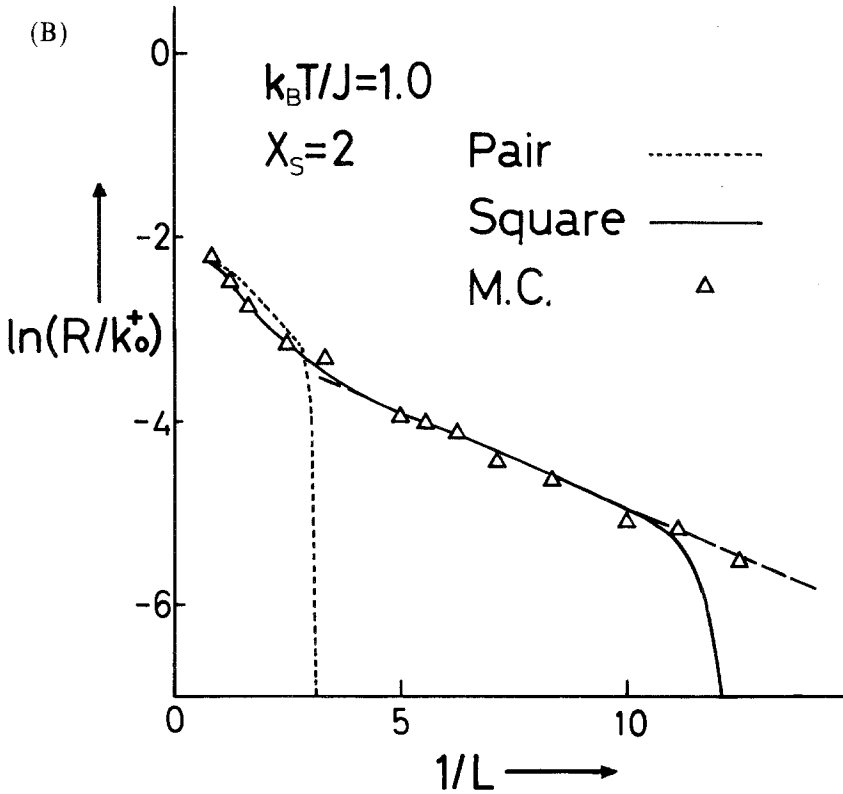


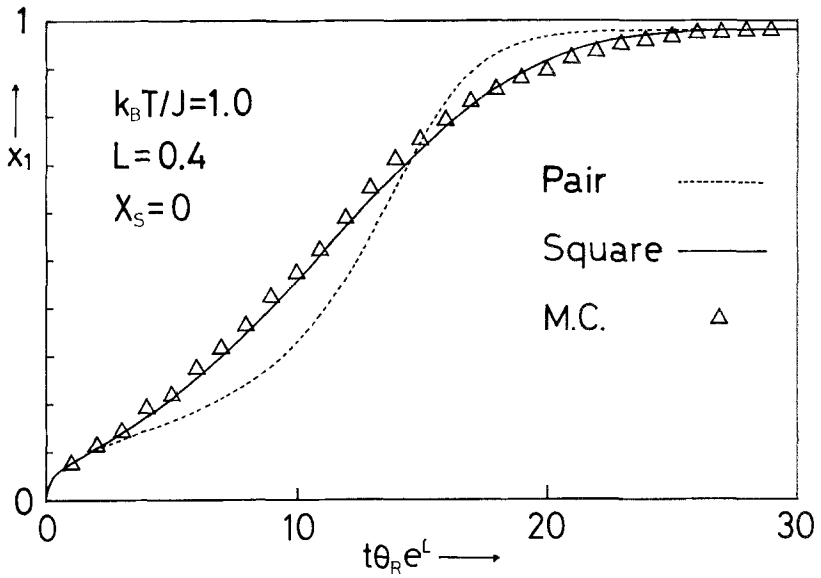
Fig. 8. (Continued)

horizontal axis is $1/L$. The data with $X_s = 2$ at the same temperature are presented in Fig. 8b. We see in both Figs. 8a and 8b that there is a wide region where the results of the square approximation agree well with those of the Monte Carlo simulation compared with those of the pair approximation. A large portion is linear and can be represented as

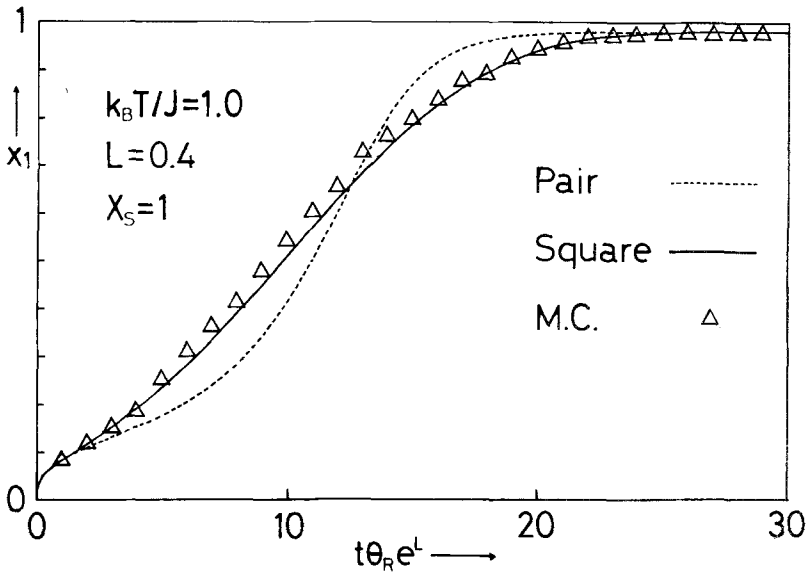
$$R = c_0 \exp(-c_1/L) \tag{4.2}$$

where c_0 and c_1 are constants. The dependence of the growth rate R on the driving force L given by (4.2) is the characteristic feature of two-dimensional nucleation-limited growth. This fact implies that even in the cluster approximation, the nucleation-limited growth phenomena can be treated if we use a basic cluster larger than the critical size of nucleation.

Figures 9a and 9b compare the details of the growth curves for the



(A)



(B)

Fig. 9. The growth curves for the pair and the square approximations together with those of the Monte Carlo simulation (40×40 lattice) in the cases (A) without diffusion ($X_S=0$) and (B) with $X_S=1$.

pair and the square approximations with those of the Monte Carlo simulation. Figure 9 clearly shows that the square approximation is an effective improvement over the pair one.

5. SUMMARY AND DISCUSSION

We have studied the static and kinetic properties of monolayer growth based on the lattice gas model in the square approximation of the CVM and the PPM. Kinetic equations for combined processes of relaxation and diffusion are obtained analytically and solved for the first time in the square approximation of the PPM. The results are compared with the point and pair approximations to see the effect of using a square as the basic cluster. The growth rate results of the square approximation are considerably improved in both cases with and without diffusion and agree well with the Monte Carlo simulation except at extremely low driving forces $L = \Delta\mu/k_B T$. The unphysical nongrowth region also shrinks considerably in the square approximation compared with that in the point and the pair ones. This is related to the static result in the CVM in which the region of metastable states shrinks as the approximation improves.

In the range where the agreement is good, there exists a region where the results of the square approximation show the characteristic feature of nucleation-limited growth. This fact implies that even in the cluster approximation method, nucleation-limited growth phenomena can be treated if we make use of a basic cluster with a size larger than the critical size of nucleation at a given temperature T and driving force L .

Our study here shows that as the size of the basic cluster becomes larger, improved results are obtained in the PPM as in the CVM. It is also noteworthy that the analytic expression of the kinetic equations for relaxation and diffusion are derived in the square approximation, since the closed-form expression for diffusion in the square approximation of the PPM has been considered very difficult in spite of the fact that the approximations with larger basic clusters such as tetrahedra and octahedra⁽⁹⁾ are often used in the CVM. We also add a comment that the possibility of using a basic cluster larger than a pair could shed light on other problems, such as the correlation factor problem in the tracer diffusion of multi-component systems; it has been argued based on comparison with Monte Carlo simulation results whether the PPM can be applied in its original form or needs a modification.⁽¹⁹⁾

APPENDIX

We show some examples of path variables here. The path variables $\{X_{ij}, Y_{ij}, Z_{ij}\}$ denote the joint probability that the cluster takes the i th state at t and the j th state at $t + \Delta t$ through a relaxation process. Examples of the path variables for the relaxation process are presented in the top row of Fig. 10. The numbers in the parentheses denote the symmetry numbers. The symmetry numbers for the path variables are summarized in Table I.

Similarly to the relaxation process, the path variables for the diffusion process are written as $\{X_{ijD}, Y_{ijD}, Z_{ijD}\}$, with the subscript D meaning

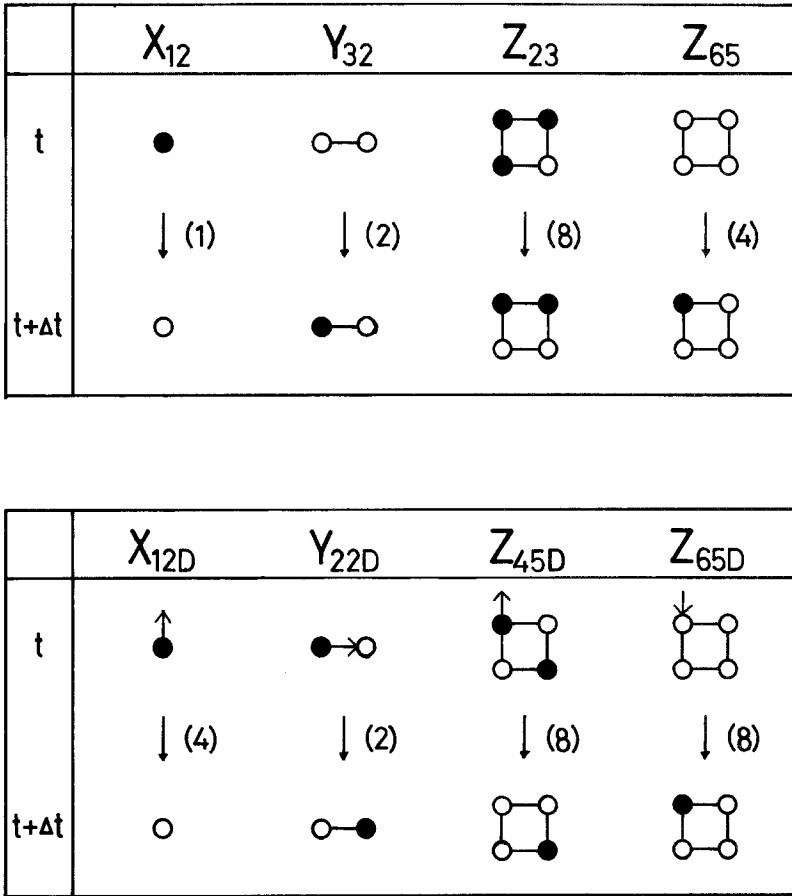


Fig. 10. Examples of path variables. The numbers in the parentheses denote the symmetry numbers.

diffusion. Y_{22D} , Z_{22D} , Z_{34D} , Z_{43D} , and Z_{55D} describe jumps of atoms within the clusters considered. On the other hand, path variables such as Z_{45D} or Z_{65D} describe jumps of atoms from or into the clusters considered, as shown in the bottom row of Fig. 11. In addition to the above, there are path variables which have four subscripts, such as Y_{12D1} or Z_{23D1} . The configuration changes for such variables are shown in Figs. 11 and 12.

Table I. The List of Symmetry Numbers for the Path Variables^a

B_{11}	B_{12}	B_{21}	B_{22}	B_{23}	B_{32}	B_{33}	G_{11}	G_{12}	G_{21}	G_{22}	G_{23}
1	2	2	2	2	2	1	1	4	4	4	8

G_{24}	G_{32}	G_{33}	G_{35}	G_{42}	G_{44}	G_{45}	G_{53}	G_{54}	G_{56}	G_{65}	G_{66}
4	8	4	8	4	2	4	8	4	4	4	1

A_{12D}	A_{21D}	B_{12D1}	B_{12D2}	B_{21D1}	B_{21D2}	B_{22D}	B_{23D1}	B_{23D2}
4	4	4	2	4	2	2	4	2

B_{32D1}	B_{32D2}	G_{12D}	G_{21D}	G_{22D}	G_{23D1}	G_{23D2}	G_{24D}	G_{32D1}
4	2	8	8	8	8	8	8	8

G_{32D2}	G_{34D}	G_{35D1}	G_{35D2}	G_{42D}	G_{43D}	G_{45D}	G_{53D1}	G_{53D2}
8	8	8	8	8	8	8	8	8

G_{54D}	G_{55D}	G_{56D}	G_{65D}
8	8	8	8

^a The symmetry numbers $A_{i,j}$ for the point path variables of the relaxation process are omitted here, since they are all equal to one.

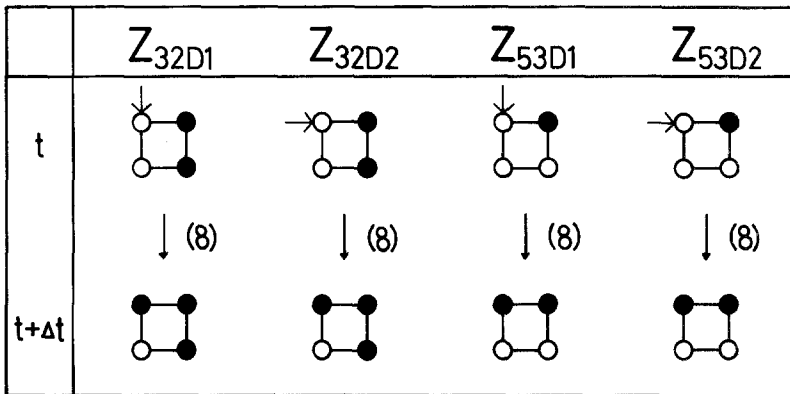
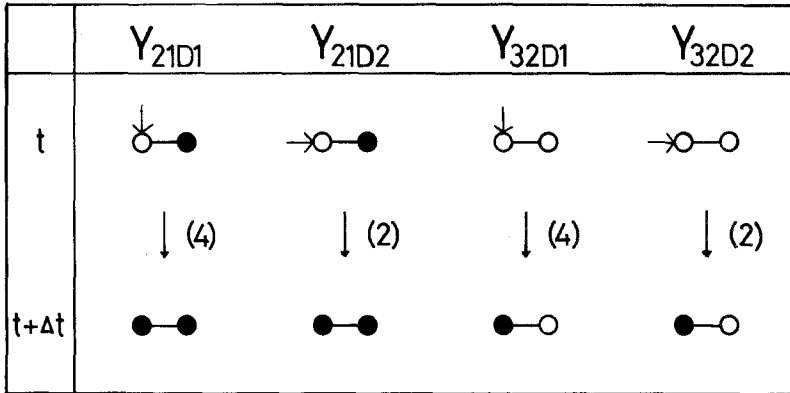


Fig. 11. The path variables for diffusion which have four subscripts. Here atoms jump into the clusters from the outside.

	Y_{12D1}	Y_{12D2}	Y_{23D1}	Y_{23D2}
t				
	↓ (4)	↓ (2)	↓ (4)	↓ (2)
$t+\Delta t$				

	Z_{23D1}	Z_{23D2}	Z_{35D1}	Z_{35D2}
t				
	↓ (8)	↓ (8)	↓ (8)	↓ (8)
$t+\Delta t$				

Fig. 12. The path variables for diffusion which have four subscripts. Here atoms jump out of the clusters to the outside.

ACKNOWLEDGMENTS

We would like to thank Prof. T. Asahi and the members of his laboratory for encouraging discussions. This work was partially supported by the Joint Research Fund of the International Scientific Research Program from the Ministry of Education, Science and Culture and also by an International Joint Research Fund from NEDO (New Energy Development Organization).

REFERENCES

1. R. Kikuchi, *Phys. Rev.* **81**:988 (1951).
2. R. Kikuchi, *Prog. Theor. Phys. (Kyoto) Suppl.* **35**:1 (1966).
3. K. Wada, M. Kaburagi, T. Uchida, and R. Kikuchi, *J. Stat. Phys.* **53**:1081 (1988).
4. D. E. Temkin, *Sov. Phys. Crystallogr.* **14** (1969).
5. R. Kikuchi, *J. Chem. Phys.* **47**:1646 (1967).
6. R. Kikuchi, *J. Chem. Phys.* **47**:1653 (1967).
7. K. Wada, H. Tsuchinaga, and T. Uchida, in *Dynamics in Ordering Processes*, S. Komura and H. Furukawa, eds. (Plenum Press, New York, 1988), p. 29.
8. T. Uchida, F. Sato, and K. Wada, *J. Crystal Growth* **99**:116 (1990).
9. J. M. Sanchez and D. de Fontaine, *Phys. Rev. B* **17**:2926 (1987).
10. R. Kikuchi, Hughes Research Laboratories Research Report no. 391 (1968).
11. R. Kikuchi, Hughes Research Laboratories Research Report no. 393 (1968).
12. W. K. Burton, N. Cabrera, and F. C. Frank, *Phil. Trans. R. Soc. Lond. A* **243**:299 (1951).
13. J. D. Weeks, G. H. Gilmer, and K. A. Jackson, *J. Chem. Phys.* **65** (1976).
14. H. Müller-Krumbhaar, *Phys. Rev. B* **14**:1308 (1974).
15. Y. Saito and H. Müller-Krumbhaar, *J. Chem. Phys.* **70**:1079 (1979).
16. G. H. Gilmer, H. J. Leamy, K. A. Jackson, and H. Reiss, *J. Crystal Growth* **24/25**:495 (1974).
17. G. H. Gilmer and P. Bennema, *J. Crystal Growth* **13/14**:148 (1972).
18. G. H. Gilmer and P. Bennema, *J. Appl. Phys.* **43**:1349 (1972).
19. H. Sato, T. Ishikawa, and R. Kikuchi, *J. Phys. Chem. Solids* **46** (1985).
20. K. Wada, T. Ishikawa, and H. Tsuchinaga, *Physica* **142A**:38 (1987).